HOSTED BY

ELSEVIER

CrossMark

Available online at www.sciencedirect.com

ScienceDirect

Progress in Natural Science: Materials International 26 (2016) 32–40

Progress in Natural Science Materials International

www.elsevier.com/locate/pnsmi
www.sciencedirect.com

Original Research

Synthesis of poly(3,4-propylenedioxythiophene)/MnO_2 composites and their applications in the adsorptive removal of methylene blue

Ruxangul Jamal[a,b], Li Zhang[a,b], Minchao Wang[a,b], Qin Zhao[a,b], Tursun Abdiryim[a,b,*]

[a]*Key Laboratory of Petroleum and Gas Fine Chemicals, Educational Ministry of China, College of Chemistry and Chemical Engineering, Xinjiang University, Urumqi 830046, China*

[b]*Key Laboratory of Functional Polymers, Xinjiang University, Urumqi 830046, China*

Received 2 February 2015; accepted 2 June 2015
Available online 11 February 2016

Abstract

The poly(3,4-propylenedioxythiophene)/MnO_2 composites (PProDOT/MnO_2) were prepared successfully by soaking the PProDOT powders into potassium permanganate ($KMnO_4$) solution, with the mass ratio of PProDOT and $KMnO_4$ from 2:1 to 1:2. The structure and morphology of composites were characterized by Fourier transform infrared spectroscopy (FTIR), Raman spectroscopy, ultraviolet–visible absorption spectra (UV), X-ray diffraction (XRD), energy-dispersive X-ray spectroscopy (EDX) and field emission scanning electron microscope (FE-SEM). Furthermore, PProDOT/MnO_2 composites were tested as the adsorbents for removal of methylene blue (MB) from aqueous solution. The results revealed that the composites were successfully synthesized, and the thiophene sulfur was oxidized into sulfoxide by $KMnO_4$. The highest percentage removal of MB after 30 min was 91% for PProDOT/MnO_2 (1:2) composite, and the percentage removal of MB was $\sim$12 mg g^{-1} after 60 min at initial concentrations of MB dye of 5.6 mg L^{-1} in the case of PProDOT/MnO_2 (1:2) composite. Besides, the adsorption process of PProDOT/MnO_2 (1:2) composite was described by pseudo-second-order and Langmuir models.

Keywords: Poly(3,4-propylenedioxythiophene); MnO_2; Composite; Adsorptive removal; Methylene blue

1. Introduction

Dyes, pigments and their related compounds are difficult for industrialization duo to their highly carcinogenic and hydrophobic property. Thus, it is significant for industry production to remove them from sewage. By now, various physic-chemical methods are used for removal of dyes, such as membrane filtration, adsorption, chemical oxidation, coagulation/flocculation, ion exchange, reverse osmosis and precipitation [1–4]. But each process has its own efficiency and limitation. In those superior methods, the adsorption has been considered as a favorable procedure due to economic feasibility, recycle of adsorbent and nonexistence of harmful residues [5–8]. Therefore, a number of the adsorbents have been developed such as activated carbon, waste materials and co-product from the agriculture as well as the waste materials from forest industries [9–13]. Among them, the waste materials and co-product ascribe to be inexpensive adsorbents since they exist in large quantities, such as, various raw agricultural solid wastes of the leaves, fibers, fruits, peels, and seeds etc. [14,15]. These adsorbents seem economically attractive for practical application. However, these adsorbents described above usually display many disadvantages involving low adsorption efficiency, long adsorption time, poor mechanical strength and the absence of specific adsorption [16]. In recent years, increasing efforts have been aimed to use polymers as adsorbents for the removal of dye from aqueous solution owing to their vast surface area, perfect mechanical rigidity, adjustable surface chemistry and pore size distribution, and feasible regeneration under mild conditions [16]. For example, Ayad et al. confirmed that polyaniline nanotubes base was employed as an efficient adsorbent for the removal of

*Corresponding author. Tel./fax: +86 991 8583575.
E-mail address: tursunabdir@sina.com.cn (T. Abdiryim).
Peer review under responsibility of Chinese Materials Research Society.

http://dx.doi.org/10.1016/j.pnsc.2016.01.001

cationic dyes such as methylene blue (MB) from aqueous solution [17]. Cassella et al. used flexible polyurethane foams as selective absorbents for MB [18]. However, a novel and efficient adsorbent based on polymer materials for removal of dyes from wastewater is still an interesting research topic.

The findings from previous research show that nanosized metal oxides (ferric oxides, aluminum oxides, titanium oxides, manganese oxides) are highly promising in adsorption process due to their affinities towards impurities and higher surface area per unit volume [19]. Among these metal oxides, MnO_2 as adsorbent has also been widely used as an effective adsorbent in the removal of heavy metals from aqueous solutions due to its high adsorption capacity and selectivity [20]. Fei et al. investigated that MnO_2 with hierarchical hollow nanostructures had a good ability to remove pollutant in waste water [21]. Cao et al. prepared γ-MnO_2/α-MnO_2 ellipsoids with an excellent ability to remove heavy metal ions and organic pollutants [22]. Recently, polymer/metal oxide hybrid adsorbents have emerged as a new class of adsorbent materials for deep removal of trace pollutants from waters. Li et al. reported that the polypyrrole/TiO_2 composites were considered as a stable adsorbent for dye removal [23].

Poly(3,4-ethylenedioxythiophene) (PEDOT), as a most promising conducting polymer, is widely used as electrode materials due to its good electrical conductivity, large , pseudocapacitance, and environmental stability [24–30]. Poly (3,4-propylene-dioxythiophene) (PProDOT) has the similar structure with PEDOT, and it shows the superior properties, such as optical and electrochromic properties, higher solubility and processibility, which is resulted from chiral alkyl chain in the ProDOT [24–30]. According to the previous report, MnO_2–NP/PEDOT nanocomposite is prepared by soaking PEDOT into a potassium permanganate solution [31]. The biggest advantage of this approach is that no additional steps are needed to prepare MnO_2 particles before synthesizing the composites. This may bring some possibility of the preparation of PProDOT/MnO_2 composites by the same method.

In this work, PProDOT/MnO_2 composites with various contents of MnO_2 were successfully synthesized by simply soaking the PProDOT powder in $KMnO_4$ solution. The PProDOT/MnO_2 composites were tested as adsorbents for removal of methylene blue (MB) from aqueous solution.

2. Experimental

2.1. Materials

3,4-Propylenedioxythiophene (ProDOT) was obtained from Aldrich and used as received. All other chemicals and solvents, including anhydrous iron (III) chloride ($FeCl_3$), potassium permanganate, ethanol and chloroform, were used as received without further purification.

2.2. Synthesis of the PProDOT

The procedure for synthesis of PProDOT by typical mechanochemical method was as follows (Fig. 1): 0.4 g ProDOT monomer and 1.67 g anhydrous iron (III) chloride ($FeCl_3$) were put in a mortar with constant grinding. After 1 h, the mixture became black–green. Then the product was washed thoroughly with distilled water, ethanol and chloroform, until the filtrate was colorless. Finally, the product was dried under vacuum at 60 °C for 48 h, the composite was denoted as PProDOT.

2.3. Preparation of PProDOT/MnO_2 composite

The procedure for synthesis of PProDOT/MnO_2 composites was as follows (Fig. 1): 0.08 g PProDOT powders put into 0.04 g $KMnO_4$ aqueous solution with magnetic stirring at room temperature, and the MnO_2 was generated in the process. After 10 min, the products were rinsed with deionized water for several times. Finally the products were dried under vacuum (60 °C) for 24 h. These products were denoted as PProDOT/MnO_2 (2:1). The loading amount of MnO_2 was controlled by changing the mass ratio of PProDOT/$KMnO_4$. The PProDOT/MnO_2 (1:1) and PProDOT/MnO_2 (1:2) composites were synthesized by the same method but only change the mass ratio of PProDOT/$KMnO_4$ = 1:1 and 1:2, respectively.

2.4. Characterization

The Fourier transform infrared (FT-IR) spectra of the samples were measured on a BRUKER EQUINOX-55 Fourier transform infrared spectrophotometer (Bruker, Billerica, MA, USA). Raman spectra of the samples were carried out a backscattering geometry with the 1064 nm excitation wavelength using a Bruker Vertex 70 FT Infrared Spectrometer. UV–vis spectra of the samples were recorded on a UV–visible spectrophotometer (UV4802, Unico, USA). The XRD patterns were conducted using a Bruker AXS D8 diffractometer and the scan range (2θ) was 10–80°, with monochromatic CuKα radiation source ($\lambda = 0.15418$ nm). The energy-dispersive X-ray spectroscopy (EDX) was taken on a Leo1430VP microscope with operating voltage 5 kV. FESEM was investigated by using Hitachi S-4800 field emission scanning electron microscope.

2.5. Adsorption experiments

For adsorption experiments, the concentrations of methylene blue solutions (MB) were determined with the absorbance at 664 nm by using UV–visible spectrophotometer (UV4802, Unico, USA). 16 mg of adsorbents (PProDOT) was shaken in MB solution (40 mL) and stirred for 120 min in the dark at 25 °C. After adsorption of dye, the adsorbents were removed by centrifugation. The adsorption study of PProDOT/MnO_2 composites was conducted by the same method.

3. Results and discussion

3.1. FTIR spectroscopy

Fig. 2(A) shows the FTIR spectra of PProDOT and PProDOT/MnO_2 composites. As seen in Fig. 2(A), the characteristic absorption bands of the pure PProDOT were at

1488, 1316, 1176, 1126, 1042, 921, 837 and 704 cm^{-1}, respectively. The bands of 1488 cm^{-1} and 1316 cm^{-1} were originated from the C=C stretching in polythiophene. Moreover, the bands at about 1176, 1126 and 1042 cm^{-1} were assigned to the C–O–C bond stretching in ethylenedioxy group. The bands at 921, 837 and 704 cm^{-1} were originated from the C–S–C bond in the thiophene ring [32–34]. After formation of the PProDOT/MnO_2 composites, several absorption bands were observed around 3380, 1620, 1044, 714 and 495 cm^{-1}, respectively. The band at around 3380 cm^{-1} and 1620 cm^{-1} is attributed to stretching and bending vibrations of the –OH group of crystal and adsorbed water molecules, respectively, which plays a very important role in the adsorption of MB [35]. Moreover, two bands at 500 cm^{-1} and 714 cm^{-1} were originated from the Mn–O and Mn–O–Mn vibrations, indicating that the MnO_2 existed in composites [36–39]. Significantly, the band at 1044 cm^{-1} gradually appeared as the ratio of MnO_2 increased in the composites, which is resulted from the sulfoxide (S=O bond) stretching mode [31]. This phenomenon reveals the thiophene sulfur may be oxidized into sulfoxide by $KMnO_4$.

3.2. Raman spectra

The Raman spectra of PProDOT and PProDOT/MnO_2 composites are presented in Fig. 2(B). As shown in Fig. 2 (B), several characteristic bands at 1537, 1410, 1237 and 1110 cm^{-1} were presented in PProDOT. The bands of 1537, 1410, 1237 and 1110 cm^{-1} are attributed to the asymmetric stretching $C_\alpha=C_\beta$, symmetric stretching $C_\alpha=C_\beta$ (–O) on five-membered ring, $C_\alpha=C_\alpha$ inter-ring stretching and C–O–C deformation, respectively [40,41]. Moreover, the characteristic bands of PProDOT/MnO_2 composites were similar to that of PProDOT. However, the MnO_2 in the composites did not display any obvious characteristic band for proving the existence of MnO_2. As it is reported that the characteristic band for MnO2 is ~570 and ~630 cm^{-1} resulted from Mn–O vibration (Raman excitation line is λ_{exc}=632.8 nm and 488 nm, respectively) [39,42]. The intensity and peak position for characteristic bands in Raman spectrum are related to the excitation wavelength [43]. In the present case, the Raman excitation line for recording the Raman spectrum is λ_{exc}=1064 nm. Therefore, the absence of obvious band for Mn–O vibration is assigned to that the lower energy of λ_{exc}=1064 nm line, which is not extremely sensitive toward the presence of MnO_2 structure in polymer matrix.

3.3. UV–vis spectroscopy

Fig. 2(C) shows the UV–vis absorption spectra of the PProDOT and PProDOT/MnO_2 composites. The PProDOT shows three characteristic absorption peaks at 430 nm, 463 nm and 487 nm, which are attributed to the π–π* transition of the thiophene ring [44,45]. These peaks are originated from the absorption peak causing by the different conjugated segments. The further comparison indicates that PProDOT/MnO_2 composites have the similar absorption peaks to that of PProDOT. Moreover, the absorption peaks of composites at 430 nm and 487 nm become sharper with an increase of loading amount of MnO_2.

3.4. XRD and EDX analysis

Fig. 3 shows the XRD patterns and EDX results of PProDOT and PProDOT/MnO_2 composites. As shown in Fig. 3, the PProDOT shows a broad and low diffraction peak at 24°, which indicates that PProDOT has an amorphous structure just like

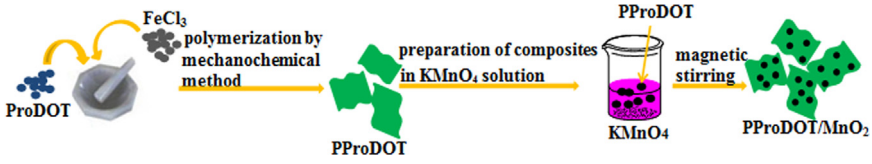

Fig. 1. Schematic diagram for the preparation of PProDOT/MnO_2 composites.

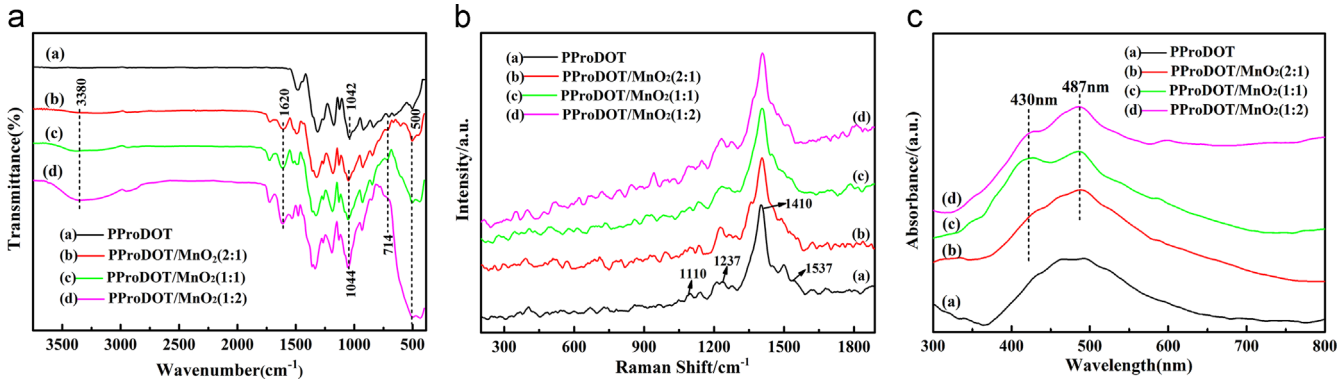

Fig. 2. The Fourier transform infrared (FTIR) spectra (A), Raman spectra (B) and ultraviolet–visible (UV–vis) spectra (C) of PProDOT and PProDOT/MnO_2 composites.

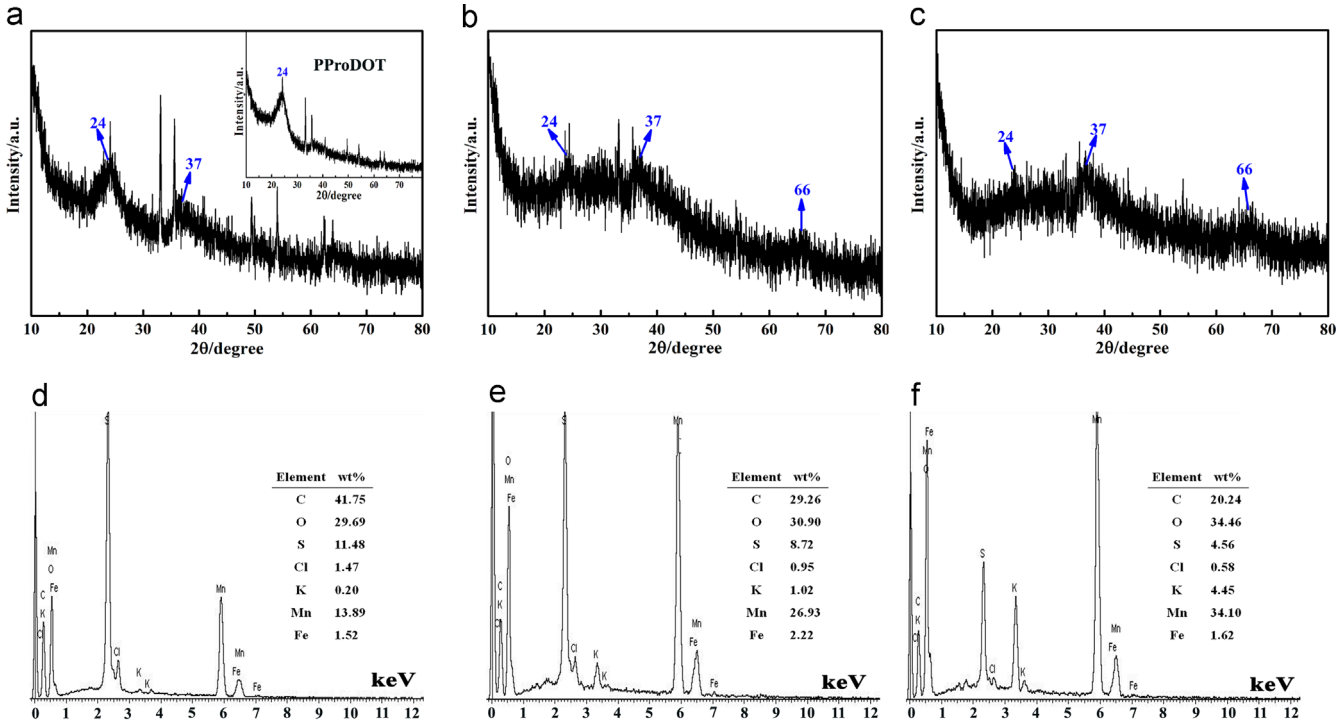

Fig. 3. X-ray diffraction (XRD) patterns of (a) PProDOT/MnO_2 (2:1), (b) PProDOT/MnO_2 (1:1), (c) PProDOT/MnO_2 (1:2) and energy dispersive X-ray spectroscopy (EDX) spectra of (d) PProDOT/MnO_2 (2:1), (e) PProDOT/MnO_2 (1:1) and (f) PProDOT/MnO_2 (1:2). The inset in panel shows the XRD pattern of PProDOT.

some other polythiophene derivatives [46–48]. Several diffraction peaks at 33°, 35°, 49°, 54° are presented in PProDOT, which is ascribed to the doping agent of $FeC1_4^-$ [34]. In the case of PProDOT/MnO_2 composites, two broad diffraction peaks are observed at 37° and 66°, which is attributed to MnO_2. The XRD pattern of MnO_2 in the composites shows broad and low peaks, indicating a poorly crystalline phase of MnO_2 [49–52]. In order to investigate the percentage of Mn element in the composites, EDX of the composites is presented in Fig. 3. Cl and Fe elements in all composites are originated from the doping agent of $FeC1_4^-$, which is agree with the results of XRD. The results also show that the percentage of Mn in the composites increases as the mass ratio of PProDOT/$KMnO_4$ varying from 2:1 to 1:2.

3.5. SEM studies

Fig. 4 shows the SEM images of the pure PProDOT and PProDOT/MnO_2 composites. As seen in Fig. 4(a)–(d), the pure PProDOT displays an irregular sponge-like morphology, and the addition of MnO_2 has some effect on the morphology of composites. As shown in Fig. 4(b)–(d), in the case of PProDOT/MnO_2 composites, many spherical particles were observed on the surface of polymer (the diameter in the range of 30–60 nm), which connects with each other resulting in a high specific surface. Such structure is conducive to contact with methylene blue molecules in the adsorption process, resulting in an improvement the adsorption efficiency. It is interesting that the decreasing of mass ratio of PProDOT/$KMnO_4$ leads to a gradual decrease in size of MnO_2 particles in composites. This phenomenon is understood by the more effective reduction of $KMnO_4$ by PProDOT in the case of low mass ratio of PProDOT/$KMnO_4$, which is beneficial for the uniform distribution of PProDOT in $KMnO_4$ solution. Consequently, the low mass ratio of PProDOT/$KMnO_4$ causes the formation of less aggregated nano-sized MnO_2 particles by initial nucleation of MnO_2 crystal. Increasing mass ratio of PProDOT/$KMnO_4$, the MnO_2 nanoparticles form initially may serve as nucleation sites for additional MnO_2 nanoparticles to cause an increase in size of MnO_2 nanoparticles in the composites.

3.6. Adsorption experiment

Fig. 5 shows the adsorption of MB (3.7 mg L^{-1}) into PProDOT and PProDOT/MnO_2 composites in the dark at 25 °C. As shown in Fig. 5, the time-resolved adsorption spectra of PProDOT and PProDOT/MnO_2 composites were analyzed by using UV–visible spectroscopy. No shifts of the characteristic peaks with increased contact time were observed, indicating that no intermediate was generated during the interaction of MB dye molecules with PProDOT/MnO_2 composites, and the decrease of peak intensity is attributed to the adsorption of MB dye molecules on the surfaces of PProDOT/MnO_2 composites [53,54]. The comparison shows that PProDOT/MnO_2 composites induce obviously decreases in the absorbance of MB. The amount of adsorbed MB onto the adsorbent, Q_e (mg g^{-1}), was calculated by the equation [55,56]:

$$Q_e = (C_o - C_e)Vm^{-1} \quad (1)$$

where

C_o: initial liquid phase dye concentration (mg L^{-1}),

C_e: equilibrium liquid phase dye concentration (mg L^{-1}),

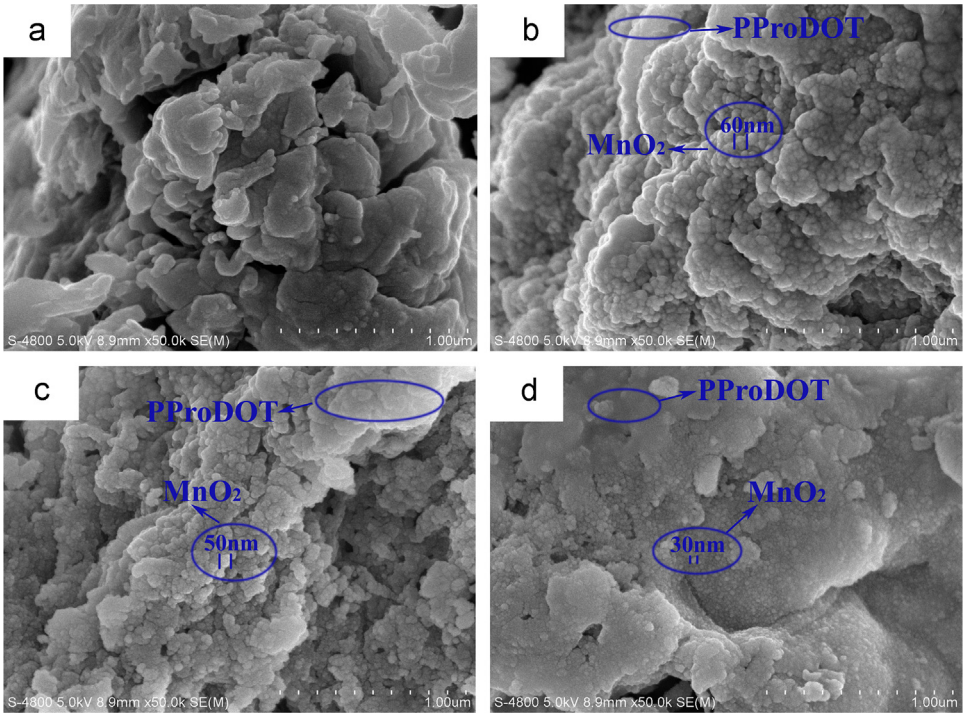

Fig. 4. Field emission scanning electron microscope (FESEM) images of (a) PProDOT, (b) PProDOT/MnO_2 (2:1), (c) PProDOT/MnO_2 (1:1) and (d) PProDOT/MnO_2 (1:2).

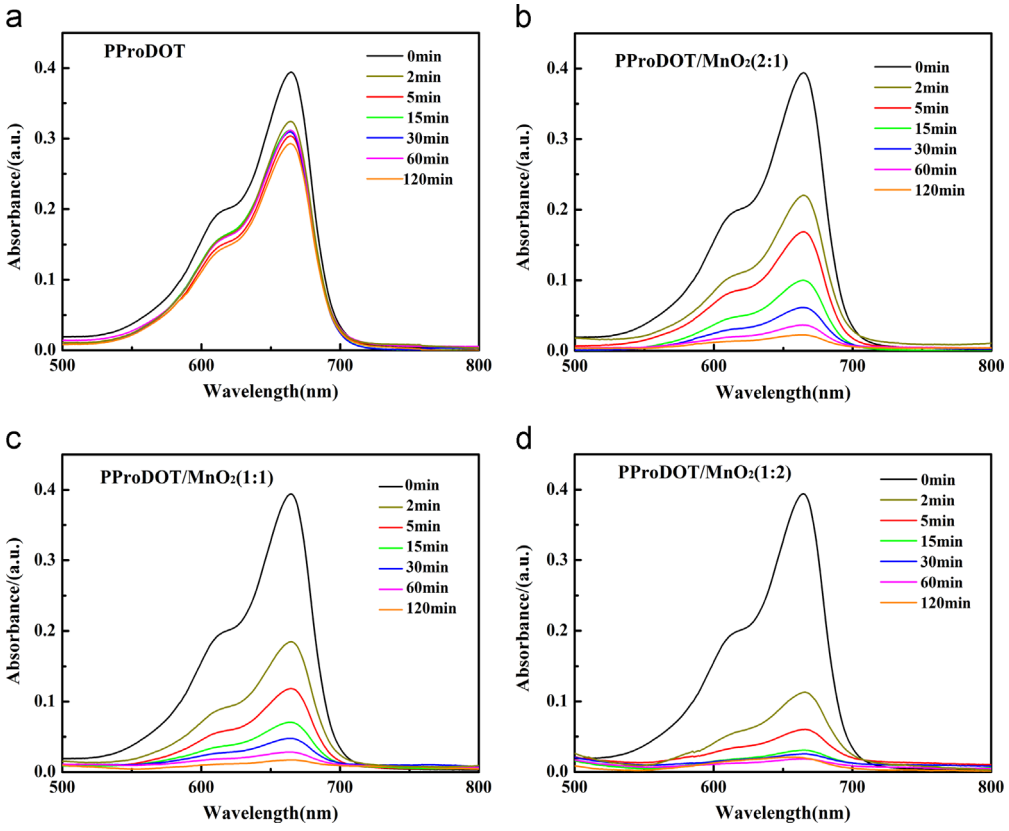

Fig. 5. Time-resolved absorption spectra of MB dye with (a) PProDOT, (b) PProDOT/MnO_2 (2:1), (c) PProDOT/MnO_2 (1:1) and (d) PProDOT/MnO_2 (1:2) in dark at 25 °C.

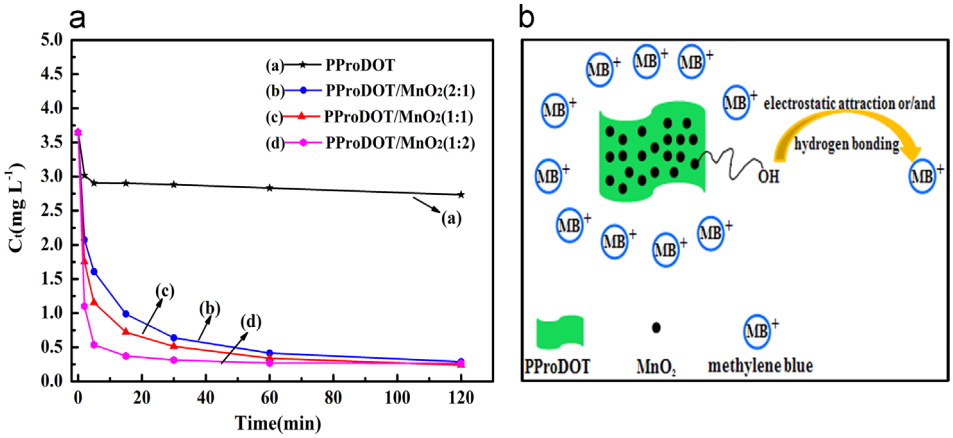

Fig. 6. Concentration profiles of MB with different time in the presence of PProDOT and PProDOT/MnO_2 composites (A); the possible mechanism for the adsorption of MB by PProDOT/MnO_2 composites (B).

V: volume of dye solution used (L),

m: mass of adsorbent used (g).

Fig. 6(A) shows the concentration profiles of MB dye with different time in the presence of PProDOT and PProDOT/MnO_2 composites. As shown in Fig. 6(A), the percentage removal of MB at initial 5 min is 21% (PProDOT), 56% (PProDOT/MnO_2 (2:1)), 69% (PProDOT/MnO_2 (1:1)), and 82% (PProDOT/MnO_2 (1:2)), respectively, while the percentage removal of MB after 30 min is 21% (PProDOT), 81% (PProDOT/MnO_2 (2:1)), 88% (PProDOT/MnO_2 (1:1)) and 91% (PProDOT/MnO_2 (1:2)), respectively. Cheng et al. reported that the percentage removal of MB by β-MnO_2 nanopincers and commercial β-MnO_2 particles was 4.2% and 2.3% after adsorption for at 30 min, respectively, and the percentage removal of MB was 30.9% after 2 min and 90.2% after 120 min in the presence of the β-MnO_2 nanopincers and H_2O_2 [57]. Wang et al. reported that the percentage removal of MB by manganese dioxide/polystyrene nanocomposite was 39.9% in 8 min [58]. This means that the PProDOT/MnO_2 composites are more effective in short adsorption time (~30 min) than these absorbents. In the present study, the percentage removal of MB on PProDOT/MnO_2 composites was higher than PProDOT at the same time in the process of adsorption. Besides, it is pointed out that the adsorption efficiency of PProDOT/MnO_2 composites increases as the mass ratio of PProDOT/$KMnO_4$ varying from 2:1 to 1:2, and the adsorption efficiency of PProDOT/MnO_2 (1:2) composite finally reaches 93% at 120 min. Compared with commercial MnO_2, PProDOT/MnO_2 composite shows better adsorption efficiency [22].

The amounts adsorbed into the PProDOT and PProDOT/MnO_2 composites are determined to be 2.28 mg g^{-1} (PProDOT), 8.08 mg g^{-1} (PProDOT/MnO_2 (2:1)), 8.26 mg g^{-1} (PProDOT/MnO_2 (1:1)), 8.45 mg g^{-1} (PProDOT/MnO_2 (1:2)), respectively. The PProDOT/MnO_2 composites exhibit higher adsorption capacity than pure PProDOT. Obviously, PProDOT/MnO_2 (1:2) displays the highest adsorption capacity (8.45 mg g^{-1}) among the composites. The better adsorption ability of PProDOT/MnO_2 composites is resulted from the strong electrostatic attraction between the surface hydroxyl groups and the cationic groups ($R–S^+$) of MB. The removal of MB is resulted from hydrogen bonding which formed by hydroxyl groups and nitrogen atoms of MB. The possible mechanism for the adsorption of MB by PProDOT/MnO_2 composites is shown in Fig. 6(B).

In order to investigate the kinetic adsorption mechanism of PProDOT/MnO_2 (1:2), the characteristic constants of adsorption were determined using the pseudo-first-order and pseudo-second-order models [59–62]. Fig. 7(a) and (b) shows the pseudo-first-order and pseudo-second-order models for adsorption of MB on PProDOT/MnO_2 (1:2).

The equation of pseudo-first-order kinetic model is as follows:

$$\log(Q_e - Q_t) = \log Q_e - t\frac{k_1}{2.303} \quad (2)$$

where

Q_e: amounts of dye adsorbed on adsorbent at equilibrium (mg g^{-1}),

Q_t: amounts of dye adsorbed on adsorbent at any time t (mg g^{-1}),

k_1: rate constant of first-order adsorption (min^{-1}).

Fig. 7(a) displays the curve-fitting plot of Eq. (2) (log ($Q_e - Q_t$) versus t). The values of k_1, Q_e and R^2 are listed in Table 1. And the correlation coefficient (R^2) of curve-fitting plots equals 0.96302.

The pseudo-second-order kinetic model equation is represented as follows:

$$\frac{t}{Q_t} = \frac{1}{k_2 Q_e^{\,2}} + \frac{1}{Q_e}t \quad (3)$$

where

k_2: rate constant of second-order adsorption (g mg^{-1} min^{-1}).

Fig. 7(b) shows the curve-fitting plot of Eq. (3) (t/Q_t versus t). The values of k_2, Q_e and R^2 are listed in Table 1. The correlation coefficient of curve-fitting plots equals 0.99999. The results indicate that MB dye adsorption on PProDOT/MnO_2 (1:2) is well-described by the pseudo-second-order kinetic model.

The most useful adsorption models of Langmuir and Freundlich are used to fit the experimental data [63,64]. Fig. 7(c) and (d) shows the Langmuir isotherm and Freundlich isotherm models for adsorption of MB on PProDOT/MnO_2 (1:2) composite.

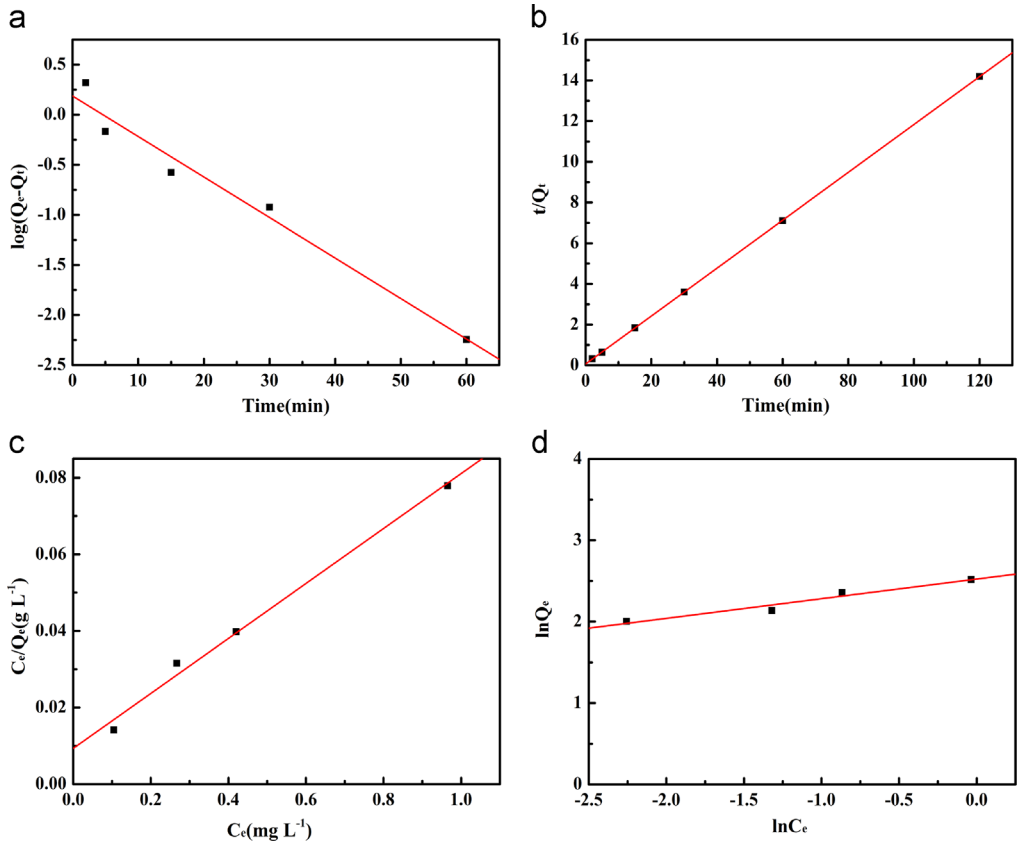

Fig. 7. (a) Pseudofirst-order and (b) pseudosecond-order models for adsorption of MB on PProDOT/MnO_2 (1:2); (c) Langmuir isotherm model and (d) Freundlich isotherm model.

The Langmuir isotherm equation is represented as follows:

$$\frac{C_e}{Q_e} = \frac{1}{Q_o} C_e + \frac{1}{K_1 Q_o} \tag{4}$$

where

Q_e: amount of adsorbed per unit mass of adsorbent (mg g^{-1}),

C_e: liquid phase dye concentration at equilibrium (mg L^{-1}),

K_1: Langmuir adsorption constant related to the energy of adsorption (L mg^{-1}),

Q_o: maximum adsorption capacity and energy of adsorption.

As shown in Fig. 7(c), a linear plot is gained when C_e/Q_e is plotted versus C_e. The unknown parameters were calculated from the intercept $[1/K_1Q_o]$ and the slope of the line $[1/Q_o]$. The correlation coefficient (R^2) equals 0.98793.

The Freundlich isotherm equation is represented as follows:

$$\ln Q_e = \ln K_f + \frac{1}{n} \ln C_e \tag{5}$$

where

K_f: Freundlich constants (L mg^{-1}),

$1/n$: heterogeneity factor.

As shown in Fig. 7(d), a linear plot is gained when ln Q_e is plotted versus ln C_e, the unknown parameters are calculated from the intercept [ln K_f] and the slope of the line $[1/n]$. The correlation coefficient (R^2) equals 0.93015. The parameters of adsorption isotherms from Langmuir and Freundlich models are presented in Table 2.

Table 1
Kinetic parameters for the adsorption of MB on PProDOT/MnO_2 (1:2) with initial MB concentration was 3.7 mg L^{-1}.

Models	Model coefficients	R^2
Pseudo-first order	Q_e=1.537 mg g^{-1} K_1=0.09313 min^{-1}	0.96302
Pseudo-second order	Q_e=8.498 mg g^{-1} K_2=0.22 g mg^{-1} min^{-1}	0.99999

In the case of Langmuir model, the maximum adsorption of MB on PProDOT/MnO_2 (1:2) is around 13.94 mg g^{-1}. Adsorption capacity of different adsorbents for MB adsorption is presented in Table 3. As shown in Table 3, the comparison indicates that PProDOT/MnO_2 (1:2) composite displays higher adsorption capacity than some adsorbents from references.

A series of experiments were conducted with different initial concentrations of MB dyes in the presence of 16 mg of PProDOT/MnO_2 (1:2) composite for 120 min. Fig. 8 shows the effects of initial concentration and time on the adsorption of MB by PProDOT/MnO_2 (1:2) composite. As initial concentrations of MB dyes increase from 3.1 mg L^{-1} to 5.6 mg L^{-1}, the amounts of equilibrium adsorption become higher (the percentage removal of MB is ~12 mg g^{-1} after 60 min at initial concentrations of MB dye of 5.6 mg L^{-1}). This phenomenon is attributed to the

Table 2
Summary of the Langmuir and Freundlich isotherm constants.

Model	Parameters
Langmuir	Q_o=13.94 (mg g^{-1}) K_1=7.709 (L mg^{-1}) R^2=0.98793
Freundlich	K_f=12.468 (L mg^{-1}) n=4.1413 R^2=0.93015

Table 3
Adsorption capacity of different adsorbents for MB adsorption.

Adsorbents	Adsorption capacity Q_o (mg g^{-1})	References
Fly ash	5.57	[7]
Glass fibers	2.24	[8]
Clay	6.3	[6]
PANI nanoparticles	6.1	[59]
PANI nanotube base/silica composite	10.3	[60]
PANI NTs	9.21	[17]
PProDOT/MnO_2 (1:2)	13.94	This work

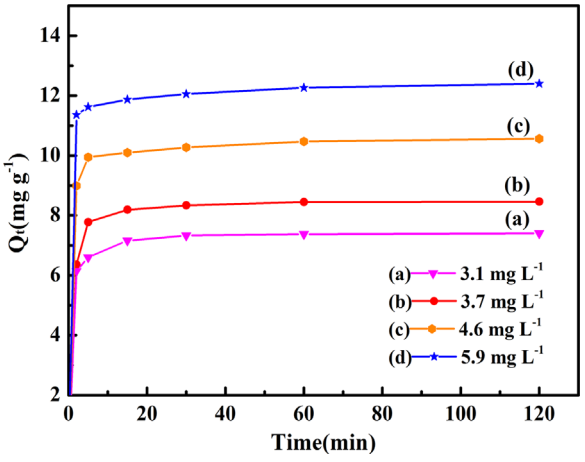

Fig. 8. Effect of initial concentration (mg L^{-1}) and time (min) on the adsorption of MB by PProDOT/MnO_2 (1:2).

mass transfer driving force enhances when the initial dye concentration increases, thereby resulting in a higher adsorption of MB. It should be noted that the percentage removal of MB by Orange peel and Banana peel is ~11 mg g^{-1} and ~7 mg g^{-1} after 60 min at initial concentrations of MB dye of 50 mg L^{-1} [65]. Therefore, it is concluded that the PProDOT/MnO_2 (1:2) composite is more effective than these natural absorbents in short adsorption time (~60 min).

4. Conclusions

In summary, PProDOT/MnO_2 composites with various contents of MnO_2 are successfully synthesized by simply soaking the PProDOT powders in $KMnO_4$ solution. The loading amount of MnO_2 is controlled by varying the mass ratio of PProDOT/$KMnO_4$. The PProDOT/MnO_2 composites are successfully synthesized by redox exchange between PProDOT and $KMnO_4$. Due to the strong electrostatic attraction or/and hydrogen bonding generated between the surface hydroxyl groups of PProDOT/MnO_2 composites and MB, the highest percentage removal of MB after 30 min is 91% for PProDOT/MnO_2 (1:2) composite, and the percentage removal of MB is ~12 mg g^{-1} after 60 min at initial concentrations of MB dye of 5.6 mg L^{-1}. The present results are well explained by pseudo-second-order kinetic model and the Langmuir adsorption isotherm. Because of the facile synthesis process and excellent adsorption performance, the PProDOT/MnO_2 composite is promising material for industrial applications.

Acknowledgments

The authors acknowledge the financial support from National Natural Science Foundation of China (Nos. 21264014 and 21464014).

References

[1] P. Bradder, S.K. Ling, S. Wang, S. Liu, J. Chem. Eng. Data 56 (2010) 138–141.
[2] P. Xiong, L. Wang, X. Sun, B. Xu, X. Wang, Ind. Eng. Chem. Res. 52 (2013) 10105–10113.
[3] Y. Anjaneyulu, N. Sreedhara Chary, D. Samuel Suman Raj, Rev. Environ. Sci. Technol. 4 (2005) 245–273.
[4] A.N. Chowdhury, S.R. Jesmeen, M.M. Hossain, Polym. Adv. Technol. 15 (2004) 633–638.
[5] G. Annadurai, M. Chellapandian, M. Krishnan, Environ. Monit. Assess. 59 (1999) 111–119.
[6] A. Gürses, S. Karaca, Ç. Doğar, R. Bayrak, M. Açıkyıldız, M. Yalçın, J. Colloid Interface Sci. 269 (2004) 310–314.
[7] K.V. Kumar, V. Ramamurthi, S. Sivanesan, J. Colloid Interface Sci. 284 (2005) 14–21.
[8] S. Chakrabarti, B.K. Dutta, J. Colloid Interface Sci. 286 (2005) 807–811.
[9] A. Bernabeu, R.F. Vercher, L. Santos-Juanes, P.J. Simón, C. Lardín, M. A. Martínez, J.A. Vicente, R. González, C. Llosá, A. Arques, A.M. Amat, Catal. Today 161 (2011) 235–240.
[10] C. Namasivayam, D. Prabha, M. Kumutha, Bioresour. Technol. 64 (1998) 77–79.
[11] A. Ramesh, D. Lee, J. Wong, J. Colloid Interface Sci. 291 (2005) 588–592.
[12] M. Ahmaruzzaman, Energy Fuels 23 (2009) 1494–1511.
[13] V. Gupta, Suhas, I. Ali, V. Saini, Ind. Eng. Chem. Res. 43 (2004) 1740–1747.
[14] M. Rafatullah, O. Sulaiman, R. Hashim, A. Ahmad, J. Hazard. Mater. 177 (2010) 70–80.
[15] D. Mohan, A. Sarswat, Y.S. Ok, C.U. Pittman Jr., Bioresour. Technol. 160 (2014) 191–202.
[16] B. Pan, B. Pan, W. Zhang, L. Lv, Q. Zhang, S. Zheng, Chem. Eng. J. 151 (2009) 19–29.
[17] M.M. Ayad, A.A. El-Nasr, J. Phys. Chem. C 114 (2010) 14377–14383.
[18] E.E. Baldez, N.F. Robaina, R.J. Cassella, J. Hazard. Mater. 159 (2008) 580–586.
[19] J.S. Markovski, V. Dokic, M. Milosavljevic, M. Mitric, A.A. Peric-Grujic, A.E. Onjia, A.D. Marinkovic, Ultrason. Sonochem. 21 (2014) 790–801.
[20] L. Bo, Q. Li, Y. Wang, L. Gao, X. Hu, J. Yang, J. Chem. Eng. 3 (2015) 1468–1475.

[21] J.B. Fei, Y. Cui, X.H. Yan, W. Qi, Y. Yang, K.W. Wang, Q. He, J.B. Li, Adv. Mater. 20 (2008) 452–456.
[22] J. Cao, Q. Mao, L. Shi, Y. Qian, J. Mater. Chem. 21 (2011) 16210.
[23] J. Li, J. Feng, W. Yan, Appl. Surf. Sci. 279 (2013) 400–408.
[24] E. Eren, G. Celik, A. Uygun, J. Tabačiarová, M. Omastová, Synth. Met. 162 (2012) 1451–1458.
[25] L. Sun, Y. Shi, Z. He, B. Li, J. Liu, Synth. Met. 162 (2012) 2183–2187.
[26] Y. Cao, T.E. Mallouk, Chem. Mater. 20 (2008) 5260–5265.
[27] H. Bejbouji, L. Vignau, J.L. Miane, M.-T. Dang, E.M. Oualim, M. Harmouchi, A. Mouhsen, Sol. Energy Mater. Sol. Cells 94 (2010) 176–181.
[28] J.I. Son, J. Hwang, S.-H. Jin, Y.-B. Shim, J. Electroanal. Chem. 628 (2009) 16–20.
[29] A. Kumar, D.M. Welsh, M.C. Morvant, F. Piroux, K.A. Abboud, J. R. Reynolds, Chem. Mater. 10 (1998) 896–902.
[30] R. Sahoo, S.P. Mishra, A. Kumar, S. Sindhu, K. Narasimha Rao, E.S. R. Gopal, Opt. Mater. 30 (2007) 143–145.
[31] R. Liu, J. Duay, S.B. Lee, ACS Nano 4 (2010) 4299–4307.
[32] H.-J. Shin, S.S. Jeon, S.S. Im, Synth. Met. 161 (2011) 1284–1288.
[33] S. Sindhu, C. Siju, S. Sharma, K. Rao, E. Gopal, Bull. Mater. Sci. 35 (2012) 611–616.
[34] T. Abdiryim, R. Jamal, C. Zhao, T. Awut, I. Nurulla, Synth. Met. 160 (2010) 325–332.
[35] I. Mohammed-Ziegler, Spectrochim. Acta A 59 (2003) 3239–3251.
[36] T.R. Bastami, M.H. Entezari, Ultrason. Sonochem. 19 (2012) 830–840.
[37] J. Han, L. Li, P. Fang, R. Guo, J. Mol. Catal. A: Chem. 116 (2012) 15900–15907.
[38] J. Safari, S. Gandomi-Ravandi, J. Mol. Catal. A: Chem. 373 (2013) 72–77.
[39] S. Maiti, A. Pramanik, S. Mahanty, ACS Appl. Mater. Interfaces (2014) 140626135117005.
[40] E. Tamburri, S. Orlanducci, F. Toschi, M.L. Terranova, D. Passeri, Synth. Met. 159 (2009) 406–414.
[41] F. Ely, A. Matsumoto, B. Zoetebier, V.S. Peressinotto, M.K. Hirata, D. A. de Sousa, R. Maciel, Org. Electron. 15 (2014) 1062–1070.
[42] T. Gao, H. Fjellvåg, P. Norby, Anal. Chim. Acta 648 (2009) 235–239.
[43] M. Baibarac, I. Baltog, S. Lefrant, J.Y. Mevellec, O. Chauvet, Chem. Mater. 15 (2003) 4149–4156.
[44] A. Ali, R. Jamal, A. Rahman, Y. Osman, T. Abdiryim, Prog. Nat. Sci.: Mater. Int. 23 (2013) 524–531.
[45] Y. Osman, R. Jamal, A. Rahman, F. Xu, A. Ali, T. Abdiryim, Synth. Met. 179 (2013) 54–59.
[46] P. Vacca, G. Nenna, R. Miscioscia, D. Palumbo, C. Minarini, D.D. Sala, J. Phys. Chem. C 113 (2009) 5777–5783.
[47] T.Y. Kim, C.M. Park, J.E. Kim, K.S. Suh, Synth. Met. 149 (2005) 169–174.
[48] M.S. Cho, S.Y. Kim, J.D. Nam, Y. Lee, Synth. Met. 158 (2008) 865–869.
[49] Y. Lv, H. Li, Y. Xie, S. Li, J. Li, Y. Xing, Y. Song, Particuology 15 (2014) 34–38.
[50] L. Athouël, F. Moser, R. Dugas, O. Crosnier, D. Bélanger, T. Brousse, J. Phys. Chem. C 112 (2008) 7270–7277.
[51] S. Devaraj, N. Munichandraiah, J. Phys. Chem. C 112 (2008) 4406–4417.
[52] H. Xia, Y. Wang, J. Lin, L. Lu, Nanoscale Res. Lett. 7 (2012) 1–10.
[53] Y. Wang, X. Zhang, X. He, W. Zhang, X. Zhang, C. Lu, Carbohydr. Polym. 110 (2014) 302–308.
[54] G. Zhao, J. Li, X. Ren, J. Hu, W. Hu, X. Wang, RSC Adv. 3 (2013) 12909.
[55] M. Özacar, Adsorption 9 (2003) 125–132.
[56] M.M. Ayad, A.A. El-Nasr, J. Phys. Chem. C 114 (2010) 14377–14383.
[57] G. Cheng, L. Yu, T. Lin, R. Yang, M. Sun, B. Lan, L. Yang, F. Deng, J. Solid State Chem. 217 (2014) 57–63.
[58] S. Wang, Z. Zhang, H. Liu, W. Zhang, Z. Qian, B. Wang, Colloid Polym. Sci. 288 (2010) 1031–1039.
[59] Y.-S. Ho, G. McKay, Process Biochem. 34 (1999) 451–465.
[60] V. Srihari, A. Das, Desalination 225 (2008) 220–234.
[61] M. Ayad, G. El-Hefnawy, S. Zaghlol, Chem. Eng. J. 217 (2013) 460–465.
[62] M.M. Ayad, A. Abu El-Nasr, J. Stejskal, J. Ind. Eng. Chem. 18 (2012) 1964–1969.
[63] A. Mellah, S. Chegrouche, Water Res. 31 (1997) 621–629.
[64] A. Al-Futaisi, A. Jamrah, R. Al-Hanai, Desalination 214 (2007) 327–342.
[65] G. Annadurai, R.-S. Juang, D.-J. Lee., J. Hazard. Mater. 92 (2002) 263–274.